RESEARCH PAPER
Contrib. Sci. & Tech Eng, 2025, 2(1)
Homepage: https://cste.journals.umz.ac.ir/
DOI: 10.22080/cste.2025.28594.1011

SARS-CoV-2 Spreading in the Indoor Environments

Amir Banari [1, 2, 3]*, Gregory Lecrivain [3], Uwe Hampel [3]

[1] *CSSB, Center for Structural Systems Biology, University of Hamburg, Germany.*

[2] *Helmholtz-Zentrum Dresden-Rossendorf, Institute of Fluid Dynamics.*

[3] *Helmholtz-Zentrum Dresden-Rossendorf, Institute of Fluid Dynamics, Germany.*

Article Info
Received 09 February 2025
Accepted 17 March 2025
Available online 17 March 2025

Keywords:
Covid-19;
Pandemic;
Cough;
Lattice Boltzmann.

Abstract:
The recent COVID-19 pandemic raises unprecedented questions regarding the spread of the SARSCoV-2 virus or any other contagion disease. How long do viruses remain in a room? How safe am I in a crowded room with poor ventilation? Will an open window decrease the risk of virus transmission in public places? A deeper understanding of drop propagation with viruses in confined environments is essential to control the recent COVID-19 pandemic and prevent the next epidemic. To address the above questions, this paper performs a numerical simulation of cough and propagation of the respiratory droplets. The effects of air conditioners and ventilation on spreading the viruses are studied, and the suspension time of the aerosols and their size will be provided.

***Corresponding Author:** amir.banari@cssb-hamburg.de

Supplementary information: Supplementary information for this article is available at https://cste.journals.umz.ac.ir/

Please cite this paper as: Banari, A., Lecrivain, G., & Hampel, U. (2025). SARS-CoV-2 spreading in the indoor environments. Contributions of Science and Technology for Engineering, 2(1), 1-11. doi:10.22080/cste.2025.28594.1011.

1. Introduction

At the time of writing of this article, more than 68 million people were COVID-19 tested positive, and 1.6 million deaths worldwide were reported. Because of the limitation of the testing, the actual cases of infected persons and casualties may be far beyond the official reports. Many countries are experiencing second or even third pandemic waves while we are approaching one year after the start of the outbreak, and again, the SARS-CoV-2 infection rate is increasing dramatically. Even one year after the pandemic, some questions remain unanswered. What is the main way in which the virus spreads? How safe is it to be in a closed environment? How do viruses spread after the infected person coughs? Is the recommended one-to-two-meter social distancing enough?

There are three main paths of virus transmission, namely surface, drop, and aerosol transmission [1]. When an infected person breathes, talks, sneezes, or coughs, drops carrying viruses are emitted with a broad size distribution [2, 3]. The larger drops fall rapidly (up to 5 seconds) to the ground or on surfaces due to gravity. These drops are largely responsible for surface and drop transmission [4].

These two types of virus transmission are avoidable by following simple hygiene protocols such as maintaining social distancing and regularly washing hands and surfaces. On the other hand, droplets in the micron range, referred to as aerosols, remain suspended much longer in the air, typically from minutes to hours. The SARS-CoV-2 transmission through these aerosols is still under debate. Bean et al. confirmed the spreading of SARS-CoV-2 via aerosols but did not express that these aerosols are viable ways to infect humans [5]. Mainly because the infection dose for COVID-19 is still unknown. Previous studies showed that some aerosols could contain enough active viruses to infect neighboring persons [6]. Not every aerosol contains active viruses. Large drops, which may contain a high amount of virus rapidly falling on the ground, are likely to contaminate. On the other hand, although only droplets with very small sizes will be suspended in the air for a long period, they are too small to contain a high dose of the virus. There exists, however, some intermediate size range in which aerosols are large enough to contain the virus and, at the same time, small enough to remain suspended and transmit the virus. Such aerosols propagate with a small airflow, allowing them to spread the virus over much greater distances [7]. In the recent COVID-19 pandemic, several cases reported in restaurants stated that the coronavirus was transmitted to people sitting even five meters away from the infected person.

Coughing is one of the main symptoms of COVID-19 disease, which plays an important role in spreading the virus

*ISSN **3060-6578***

from the infected person. Studying cough has received less attention than sneezing. Sneeze is considered more important for spreading the viruses due to its higher impact velocity, which could throw droplets to a longer distance. After sneezing, the droplet can travel and land 6 to 8 m away [8]. It is argued that coughing/sneezing produces a turbulent cloud that consists of hot and moist exhaled air and drops that remain suspended in the cloud for a long distance.

A cough's initial impact velocity is much lower than a sneeze. Nevertheless, it could produce thousands of aerosols that may transmit the disease even hours after the cough [9]. Lidslay et al. investigated cough with nine subjects with and without influenza [10]. They used a particle spectrometer with a size range of 0.35 to 10 μm. It was reported in their work that the number of particles in this size range varied widely from patient to patient and was from 900 to 302,200 particles per cough. It will be shown in section 4 of the current paper that these size droplets will become aerosols and could d be suspended in the air for a long period.

Aerosol transmission was observed more clearly during the COVID-19 outbreak in an apartment complex in Hong Kong. More than 300 people were reported infected. Rather than the random distribution you might expect from contact or droplets spread through common areas, residents on higher floors were more likely to be infected, ”consistent with a plume of contaminated warm air” [11].

Cowling et al. [12] studied the spreading of the influenza virus. They found that aerosol transmission accounts for approximately half of all transmission events. This suggests that reducing virus transmission by contact or large droplets may not be sufficient to control the virus's spreading.

The importance of aerosol virus transmission leads to a more detailed study of cough as one of the main COVID-19 diseases. In experimental cough studies, Particle Image Velocimetry (PIV) or Hot Wire Anemometry (HWA) are usually employed in a coughing person's near-mouth area or on a small box or point away from the mouth in a specific location. However, these methods fail to track the particle propagation in the entire room due to technical limitations in capturing the flow field and aerosols in the entire room. This brings the need for a numerical simulation.

Kang et al. used the Lagrangian method for particle tracking to study coughed droplets with a size of 10μm in the air conditioning room [13].

Pendar et al. applied a comprehensive, fully coupled Eulerian-Lagrangian method to study the saliva-disease-carrier droplet transmission mechanisms and track their trajectory using the OpenFOAM package [14]. In their paper, they focus mainly on sneezing rather than coughing.

A comprehensive numerical study is investigated in the current work to study the cough mechanism and how the droplets spread in a room under different conditions. A computer simulation has been performed on the propagation of respiratory fluid aerosols following a human cough. First, the flow filed after the cough is validated to the existing experimental data. Then, the propagation of the cough droplets is studied. The main focus lies on the effect of opening the room window for virus ventilating. Furthermore, the dependencies of drop behavior are given as the function of time and size. The estimated number of droplets, size, and velocity have been imported from previous experimental studies [15, 16]. Gupta et al. [17] measured the flow dynamics of coughs near the mouth. They released a model for the time history of the cough velocity at the mouth and also the mouth opening area. Their paper reported that the jet direction and mouth opening area during a cough seemed not related to the physiological parameters of the human subjects.

In this study, the lattice Boltzmann method is employed for simulating flow because of its several advantages concerning classical Eulerian/Navier-Stokes solvers. It benefits from a straightforward implementation and does not need pressure correction. The locality of the operators allows us to take full advantage of recent advances in parallel General Purpose Graphical Processing Units (GPGPU) for fast calculation [18]. A Lagrangian approach is used to track droplet propagation. The evaporation of the aerosols is neglected. Droplets' motion is governed by the drag of the airflow around small particles. This paper is organized as follows: Section 2 provides an introduction to particle-laden flow. Sections 2.1 and 2.2 describe particle tracking and fluid solver methodology. Section 3 validates the numerical tool with experimental data. Section 4 studies the spreading of the cough drops in detail. Finally, Section 5 offers conclusions and perspectives for future work.

2. Particle Laden Flow

The model described by Elghobashi [19] has been used for simulating the particle-laden flow. In this model, the particle's movement happens due to the drag force of flow around the sphere and the amount of this force per unit volume exerted in the location of the particles as a feedback body force to the flow. The particle tracking is called the dispersed phase, and the fluid solver is called the carried phase. The methodologies of these two solvers are explained below.

2.1. Dispersed Phase

All droplets in the dispersed phase are small rigid spheres. Maxey and Riley [20] made the following assumptions, which are also applied in our work:

- the particles are rigid, i.e., no deformation is allowed: the shape and dimensions of the particles remain constant,
- the particles are spherical, and no shape effects are considered.
- the particles are really small where the particle Reynolds number defined by $Re_p = d_p \mid u_{pj} - v_{pj} \mid / v$ is very small: $Re_p < 1$, so that the drag coefficient for a small sphere can be applied, where u_{pj} is the j component of the fluid velocity at the location of particle p, v_{pj} is j component velocity of particle p, and v is the kinematic viscosity of the fluid.

The governing Equation of motion for each individual particle is found in Newton’s second law. By neglecting the added mass and lift force, the Equation is

$$m_p \frac{dv_j}{dt} = D_{pj} + G_{pj} + B_{pj}(m_p - m_f)g_j \quad (1)$$

where m_p is the mass of the particle, D is the drag force, G is the gravity force, and B is the buoyancy force.

The expression of the D_{pj} term is derived from the formulation of the drag force applied on a sphere by $F_{pj} = \frac{1}{2} C_D A_p \rho_f (u_j - v_j)|u_j - v_j|. A_p$ the cross-section area of the particle, and C_D is the drag coefficient, which is a function of Re_p.

$$C_d = \frac{24}{Re_P}(1 + 0.15Re_p^{0.687}) \quad (2)$$

Replacing the above terms is in Equation 1, and with some simplification, the final form of particle motion Equation becomes:

$$\frac{dv_j}{dt} = \frac{(u_j - v_j)}{\tau_p}\left(1 + 0.15Re_p^{0.687}\right) + g_j\left(1 - \frac{\rho_f}{\rho_p}\right) \quad (3)$$
$$with\ \tau_p = \frac{\rho_p d_p^2}{18\rho_f \vartheta}$$

In Equation 3, the u_{pj}, fluid velocity in particle position, is needed at every time step. However, the LB code computes the fluid velocity on each grid node of the domain. The particles being dispersed in the flow during the simulations may not be found on grid nodes, which is the reason why an interpolation must be performed to determine the fluid velocity at the particle positions. In our case, the fluid velocity field is interpolated via a tricubic interpolation scheme developed by Lekien and Marsden [21]. This local interpolation method is based on the determination of a 64×64 matrix that relates the derivatives at the corners of an element to the coefficients of the tri cubic for this element and presents two main advantages; on one hand, it uses only the neighboring points of the element instead of the whole dataset to determine the fluid velocity, and on the other hand, a unique set of coefficients for the velocity interpolation is determined once and stored for further usage, which saves both time and computational resources. Once the carrier fluid velocity field is determined, a Taylor series expansion calculates the new particle velocity.

$$v_j^{t+1} = v_j^t + \Delta t\left(\frac{u_j^t - v_j^t}{\tau_p}\left(1 + 0.15Re_p^{0.687}\right) + g_j\left(1 - \frac{\rho_f}{\rho_p}\right)\right) + O(\Delta t^2) \quad (4)$$

The position of the particles is then derived by time integration of the velocity, again via Taylor series expansion:

$$x_{jp}^{t+1} = x_{jp}^t + \Delta t \frac{dx_{jp}}{dt} + \frac{1}{2}\Delta t^2 \frac{d^2 x_{jp}}{dt^2} + O(\Delta t^3) = x_{jp}^t + \Delta t v_j + \frac{1}{2}\Delta t^2 a_j + O(\Delta t^3) \quad (5)$$

In summary, the following steps are performed to track the particles: Interpolation of the fluid velocity *up* to find its value at the particle's position *xpj*. Equations 4 and 5 are then used to find the particle's velocity and position in a new time step. Subsequently, the term *Fpj*, s is extrapolated to the neighboring grid node and inserted as the particle's feedback effect to the fluid solver.

2.2. Carrier Phase

An efficient implementation of the Lattice Boltzmann Method is used within this study for the numerical simulation of the fluid flow. The LBM is based on the Boltzmann equation from a microscopic scale point of view. The LBM then discretizes the Boltzmann equation with a discrete velocity set, yielding a numerical method for computing macroscopic distribution functions on a Cartesian grid. The macroscopic hydrodynamic quantities, such as pressure and velocity, are obtained as low-order moments of these distribution functions. It can be shown that for sufficiently small values of space and time steps, Mach (Ma) and Knudsen (Kn) numbers, the LBM solution converges to that of the NS Equations.

The Boltzmann equation thus governs particle distribution functions (PDF), $f(x,t,\xi)$, which specify the probability of finding a fluid particle at position x at time t with (particle) velocity ξ, [22, 23]. The Boltzmann equation is

$$\frac{\partial f(x,t,\xi)}{\partial t} + \xi \cdot \frac{\partial f(x,t,\xi)}{\partial x} = \Omega \quad (6)$$

Ω is the collision operator, which describes the interaction of particles.

Discretized particle velocities e_{ijk} are introduced to yield a model of reduced computational cost. In this discretized formulation, a particle is only allowed to move from a given lattice point in a limited number of directions and for specific distances. With these assumptions, Equation 6 transforms into a set of discrete Boltzmann Equations

$$\frac{\partial fijk(x,t)}{\partial t} + e_{ijk} \cdot \frac{\partial fijk(x,t)}{\partial x} = \Omega_{ijk} \quad (7)$$

where $e_{ijk} = c\times(i,j,k)$ and $i,j,k \in (-1,0,1)$. $c = \Delta x/\Delta t$ is the lattice speed, with Δx being the regular lattice space step and Δt the time step. In the implementation of LBM, c usually gets a unity value. This means that a particle with velocity c will travel one lattice cell within a discrete time step. The definition of e_{ijk} will form a lattice with 27 discretized velocities, which is called the D3Q27 model (3 dimensional and 27 velocities, see Figure 1).

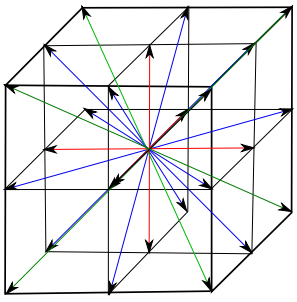

Figure 1. *D3Q27* lattice model used in the present LBM, where the vectors indicate the 27 possible velocity vectors

A finite difference discretization in space and time over a grid cell yields the lattice Boltzmann Equation

$$f_{ijk}(x + e_{ijk}\Delta t, t + \Delta t) = f_{ijk}(x,t) + \Delta t \Omega_{ijk} \quad (8)$$

Equation 8 may be split up into two parts. The first part contains the collision step, in which the particle distribution functions change from the equilibrium state due to the collision of the particles. The second part is the propagation step, in which the evolved particle distribution functions are moved to the respective neighboring grid points. The collision step is a complete local operator, and this LBM characteristic makes the numerical method highly suitable for taking advantage of GPGPU for high-performance computing.

$$\bar{f}_{ijk}(x,t) = f_{ijk}(x,t) + \Omega_{ijk} \quad \textit{Collision step} \quad (9)$$

$$f_{ijk}(x + e_{ijk}\Delta t, t + \Delta t) = \bar{f}_{ijk}(x,t) \quad \textit{Propagation step} \quad (10)$$

where $\bar{f}_{ijk}$ is the post-collision particle distribution function. A new model called the cumulant lattice Boltzmann equation has been used for the collision operator. The cumulant method has crucial advantages compared to other LBM collision operators, e.g., MRT, TRT, and BGK. The cumulant operator is Galilean invariant. Moreover, it is more stable and produces smaller errors and noises. Banari et al. [24] comprehensively explain the cumulant method. The pressure and velocities are obtained from the zeroth and first-order moments of the particle distribution functions.

$$p = c_s^2 \sum_{i=-1}^{1} f_{ijk}, \quad (11)$$

$$u = \frac{1}{\rho}\sum_{i=-1}^{1} f_{ijk}\, e_{ijk} \sum_{j=-1}^{1} f_{ijk}\, e_{ijk} \sum_{k=-1}^{1} f_{ijk}\, e_{ijk} \quad (12)$$

where $c_s = c/\sqrt{3}$ is the speed of sound in the lattice.

2.3. Grid Refinement

In the simulation of the cough, high grid resolution is needed for areas close to the mouse where high gradients exist. The memory of one single GPU for running the current simulation is not enough due to a large number of grid points. The current work has been run on the Helmholtz-Zentrum Dresden-Rossendorf (HZDR) high-performance computing cluster "Hemera" with Tesla P100 GPU. This GPU has 16 GB of memory on 2880 CUDA cores. To overcome this problem, a grid refinement technique is implemented at a high gradient area where more resolution is needed. The grid size of fine mesh is half of the grid size of coarse mesh $\Delta x_c = 2\Delta x_f$, which means that the time step in the coarse patch is twice the time step in the fine patch ($\Delta t_c = 2\Delta t_f$). Therefore, the fine patch should be solved in two time steps to reach to the same time level as the coarse patch after one time step. After the end of one coarse patch time step (two fine patch time steps), some missing particle distribution functions must be updated. These nodes are colored red in Figure 2. An interpolation scheme has to be applied to the fine-coarse boundary. The inner coarse nodes, big red nodes in Figure 2, are updated by averaging the neighboring fine nodes and unknown fine patch PDFs, and small red nodes in Figure 2 are found by a tri-linear interpolation.

After finding the values of fine (coarse) patch PDFs on the position of unknown coarse (fine) nodes, scaling of non-the equilibrium part is necessary to find the final magnitudes of

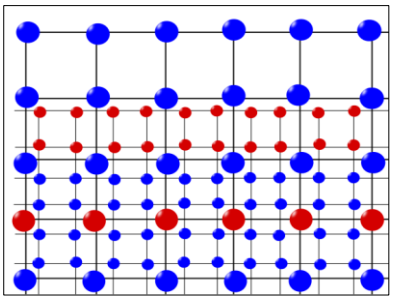

Figure 2. Invalid and valid nodes in fine and coarse grids. red (invalid), blue (valid)

unknown PDFs. The equilibrium part of PDFs for the fine and coarse patches are only functions of hydrodynamic parameters and are the same in both grids. Therefore, the unknown PDFs are calculated with

$$f_{i,c} = f_{i,f}^{eq} + r f_{i,f}^{neq} \quad (13)$$

$$f_{i,f} = f_{i,c}^{eq} + \frac{1}{r} f_{i,c}^{neq} \quad (14)$$

where $f_{i,c}$ and $f_{i,f}$ are missing PDFs in coarse and fine grid, respectively. In the Equation above, r is the scale factor coefficient between non-equilibrium PDFs of fine and coarse grids, which is defined as

$$r = \frac{\vartheta_f(6\vartheta_C + 1)}{\vartheta_c(6\vartheta_f + 1)} \quad (15)$$

where v_f and v_c are the fluid viscosity in lattice Boltzmann units for fine and coarse mesh, respectively. More details concerning the derivation of the scale factor can be found by Dudalski et al. [25].

3. Comparison to the Experimental Data

In order to check the capability of the numerical fluid solver for the simulation of the human cough, a comparison to the experimental work of Dudalski et al. [25] is performed in this section. Dudalski et al. [25] conducted Particle image velocimetry (PIV) and hot-wire anemometry (HWA) measurements at 1 m away from the mouth of human subjects. They developed a model for cough flow behavior at the far field location of the mouth, which is important for the post-cough spreading of the cough droplets. In their work, they only recorded the time history of the cough velocity field, and the cough drop propagation was not investigated (which is studied in the current work and is discussed in section 4). Cough velocity and duration are highly case-sensitive. It may vary by age, gender, and health condition of the coughing person. Dudalski et al. [25] performed 77 experiments with 58 different subjects, and the average of all recorded velocity fields is considered the final cough velocity field model.

It must be stated that in the experimental tests, although the human subject was required to cough horizontally, there was still a small angle in the cough jet flow direction. Dudalski

et al. defined the "cough jet center line" as the midpoint of the cough, where the greatest velocities are present. The "cough jet center line" is found after examining and averaging the velocity contours and vector arrays of all trials. However, for the numerical simulation, since the direction of the inlet velocity is set in the horizontal direction, the "cough jet center line" is a horizontal line from the mouth.

The computational domain that is used for the cough simulations in this work is sketched in Figure 3-a. The numerical chamber dimension is $1.8 \times 1.2 \times 1.4$ in x,y and z directions. This dimension is used to minimize the effect of the wall on the cough. A no-slip boundary condition is used at all the surfaces except the location of the mouse, where the inlet velocity boundary condition is used. The fine grid is located from the mouth to $1.2m$ away from it, where the majority of cough propagation and high gradients take place. The grid dimensions and fine and coarse grid setup are illustrated in Figure 3-b. Grid nodes of $Nx = 413$, $Ny = 229$, and $Nz = 308$ for the coarse grid and $nx = 546$, $ny = 136$, and $nz = 136$ for the fine grid are used. This grid setup gives $\Delta x_c = 0.004393m$ and $\Delta x_f = 0.002197m$ for coarse and fine grid spacing, respectively. For the inlet velocity in the mouth, the velocity profile and also the mouth size suggested by Gupta et al. [17] are used. Gupta et al. [17] determined experimentally, with several cases, the average cough flow rate and also mouth size during the cough. The mouth is considered to be circular, with a radius of $d = 0.012$. This radius is set to be in the range of the calculated average mouth size proposed by Gupta et al. [17]. Using this mouth size, the cough velocity at the mouth will be calculated from the flow rate, which is illustrated in Figure 4 as a function of the time. This cough velocity profile shows a duration of around 0.6 seconds and a maximum velocity of $vmax \sim= 22m/$e.

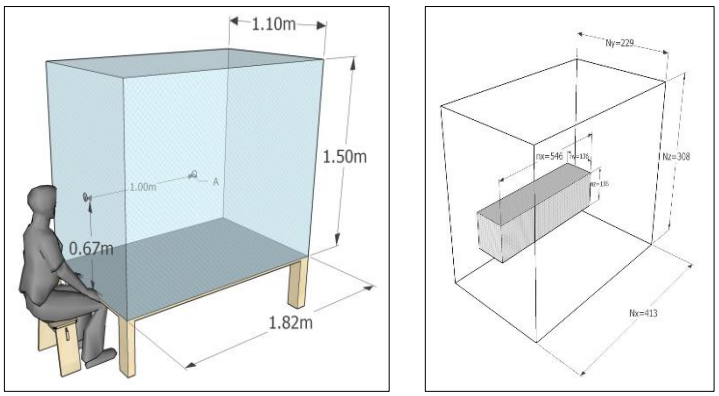

(a) (b)

Figure 3. (a) Schematic view of computational chamber dimensions, (b) Fine (gray box) and coarse grid placement in the computational grid

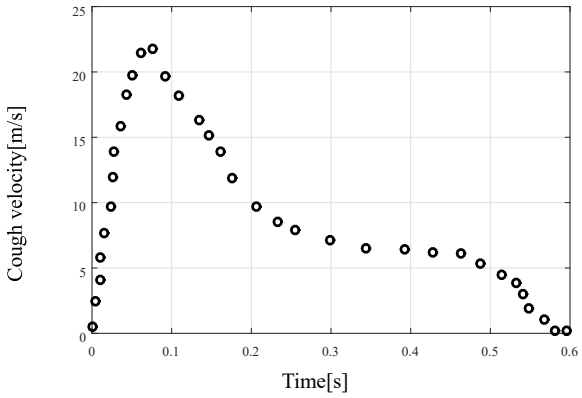

Figure 4. Cough flow rate variation with time from [17]

The LBM cough simulation is validated by comparing it to the HWA data from Dudalski et al. [25]. Figure 5-a compares LBM and HWA normalized velocity profiles as the function of normalized time at the location of point A, $x = 1m$ from mouth on jet cough center line ($x = 1m, y = 0, z = 0.67m$) (see Figure 3-a). The normalized velocity V and the normalized time t are defined:

$$\overline{V} = \frac{V(t)}{V_{peak}} \; and \; \overline{t} = \frac{t}{t_{peak}} \tag{16}$$

where $V(t) = \sqrt{u_x^2 + u_z^2}$ is 2D instantaneous velocity magnitude at point A. V_{peak} is the maximum velocity $V(t)$, and t_{peak} is the time t at which V_{peak} occurs.

The date of HWA is the average of 72 records. Also, for the LBM results, the profile is the average of 6 simulations with small random perturbation in the inlet velocity to mimic the randomness of the cough. Very good agreement is observed between the numerical and the experimental results, which shows the capability of the LBM to capture the cough flow. Moreover, in Figure 5-b, the 2D velocity magnitude is

illustrated as the function of time. The peak velocity of $V_{peak} = 0.94 m/s$ is seen in this Figure, which is slightly lower than the average peak velocity Vpeak = 1.17m/s reported by Dudalski et al. [25].

Figure 6 compares instantaneous velocity magnitude contours to Mohamed's PIV measurements [26].

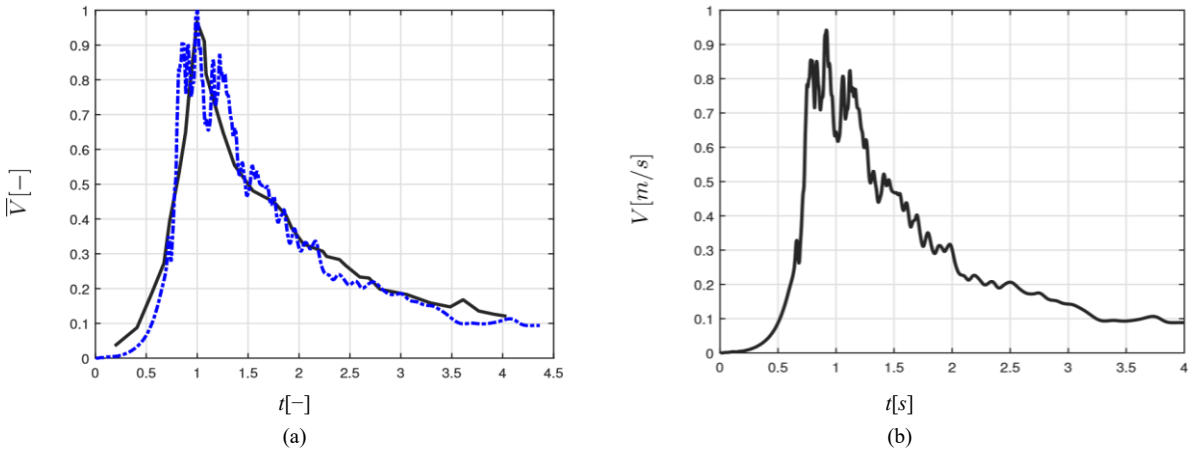

Figure 5. (a)Normalized Velocity at point A and its comparison to the experimental data of Mohamed [26], LBM result ( ), experimental data (), (b) Numerical 2D velocity magnitude at point A

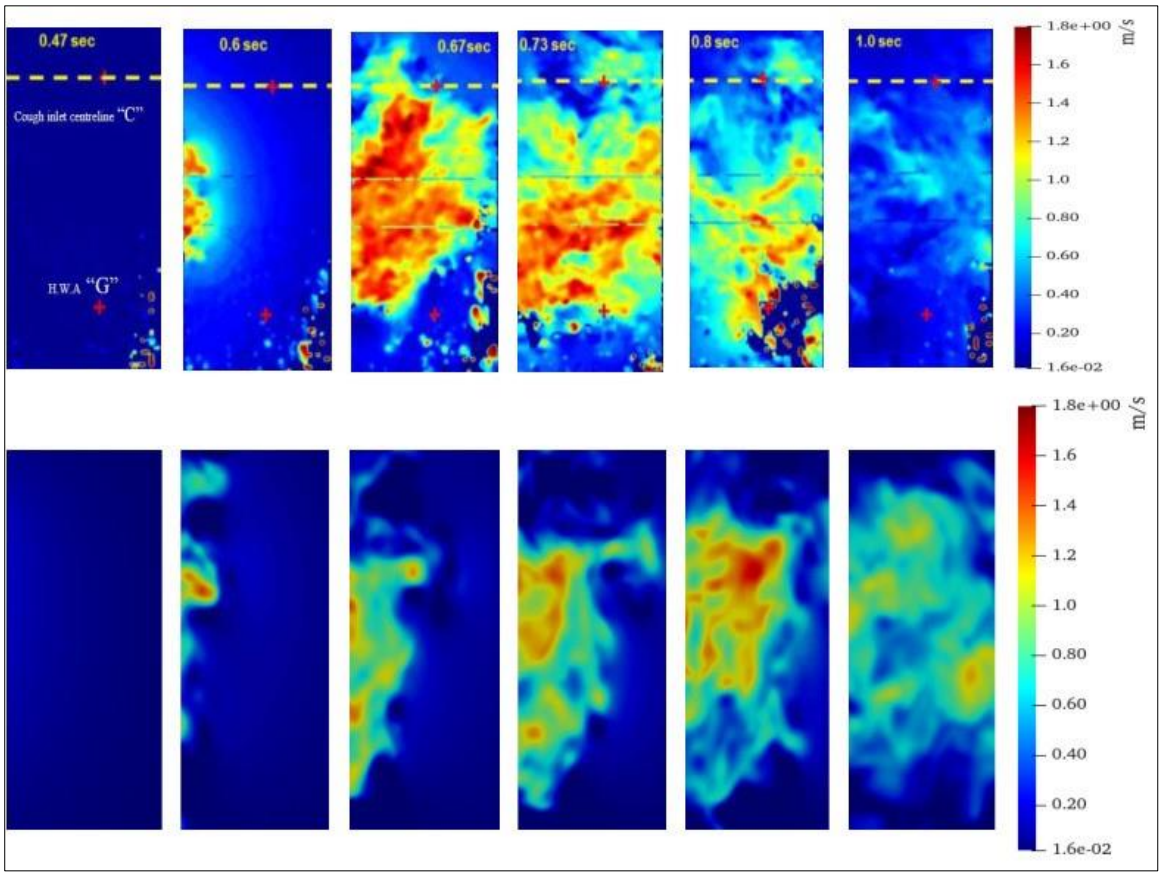

Figure 6. Comparison of instantaneous velocity magnitude to the PIV measurements of Mohammad et al.

The experimental chamber setup of Mohamed [26] is the same as Dudalski et al. [25]. The PIV velocity contours are computed in a rectangular field view with the dimension of 0.14cm by 0.34cm around the cough jet center line. The noises at the lower right corner of the field of view of PIV measurements are affected by camera malfunction. This comparison shows qualitatively the effectiveness of the inlet velocity boundary condition and the numerical simulation. The cough jet enters the field view at 0.6 seconds, and the maximum velocity and counters match the PIV data.

Furthermore, the instantaneous velocity magnitude in the whole domain is shown in Figure 7, and the spread of the cough early after the impact is illustrated in Figure 8. These figures help to provide a better understanding of the dynamics of the cough. In Figure 7, for the times $t = 2,3,4s$, a high-velocity pocket can be observed at the front of the jet that separates it from the rest of the jet. This high-velocity pocket contains the main energy of the cough while the rest of the jet speed decays in the early stage. This incident was also observed in some experimental works in which a high-

speed cloud containing thousands of drops was observed. This cloud is responsible for spreading the virus much further than expected. More details about this phenomenon are explained in section 4.

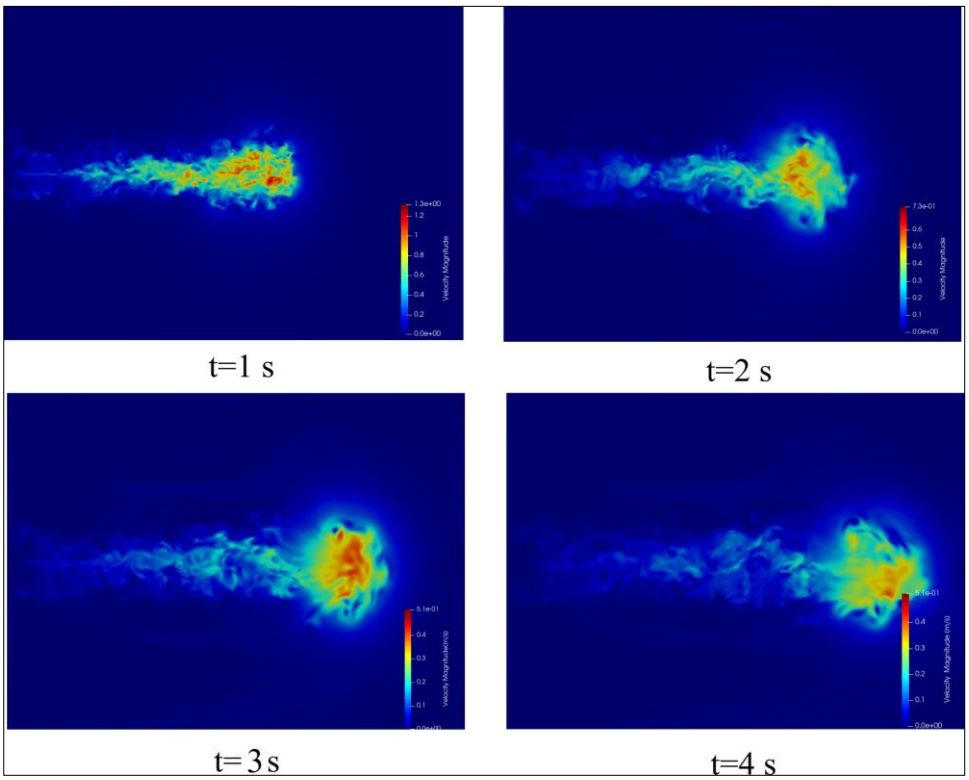

Figure 7. **Instantaneous velocity magnitude of the cough jet**

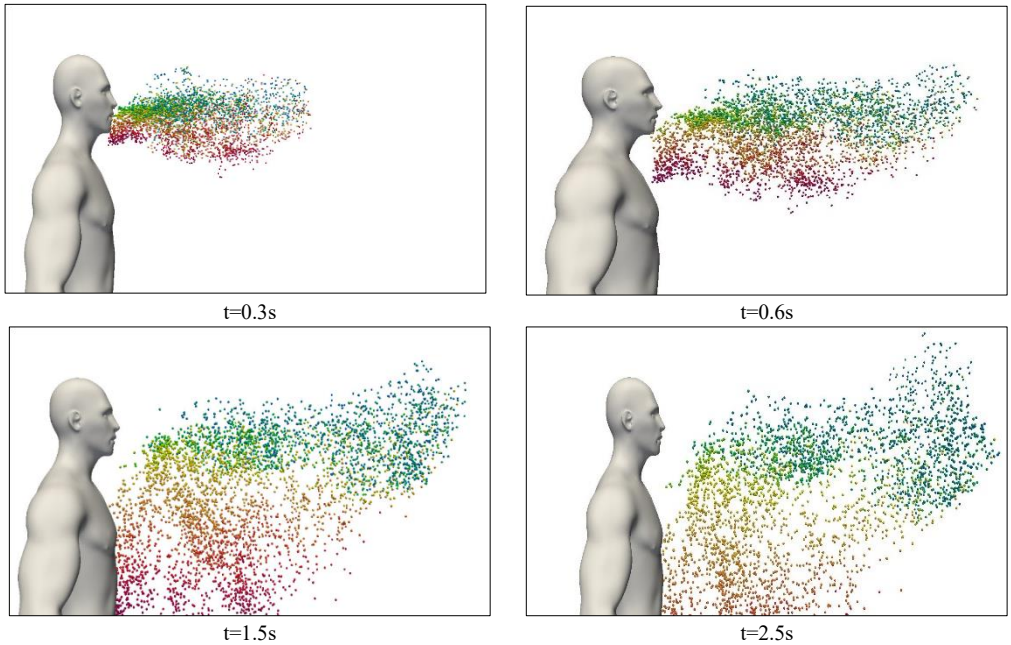

Figure 8. **Drops spreading early after the cough**

4. Cough Drops Spreading in a Room

This section carries out a numerical simulation of the cough spreading in a room to investigate the virus spreading in a confined environment.

The room size is $5m \times 2.6m \times 2.6m$. A person with a height of $1.75cm$ is standing next to the wall. Gupta cough velocity is implemented. Four thousand particles are inserted into the mouse with random diameter sizes in the range of $7\mu m$ to $100\mu m$. Also, an air conditioner blows at a very low speed in the room. Although the AC speed is low, it is high enough to spread the small droplets throughout the room.

For the first study, the average size of the droplets falling on the ground and the horizontal spreading quickly after the cough are investigated. In the left panel of Figure 9, droplets are projected on an $x-z$ plane, and their 2D velocity vector is illustrated. In the right panel of Figure 9, the average size

of particles falling on the ground as the function of horizontal distance from the mouth is plotted. For the time t = 5sec, particles with a diameter around d = 9.4μm fell on the ground up to a distance of x = 1.6m away from the mouth. For the time t = 10,20,40sec, particles fell on the ground up to a distance of x = 1.8,2.0,2.2m away from the mouth, respectively. Moreover, from the left panel of Figure 9, the maximum horizontal spreading of the cough drops can be observed. For the time t = 5,10,20,40 sec, drops travel up to a distance of x = 2.1,2.5,3.0,3.5m away from the mouth.

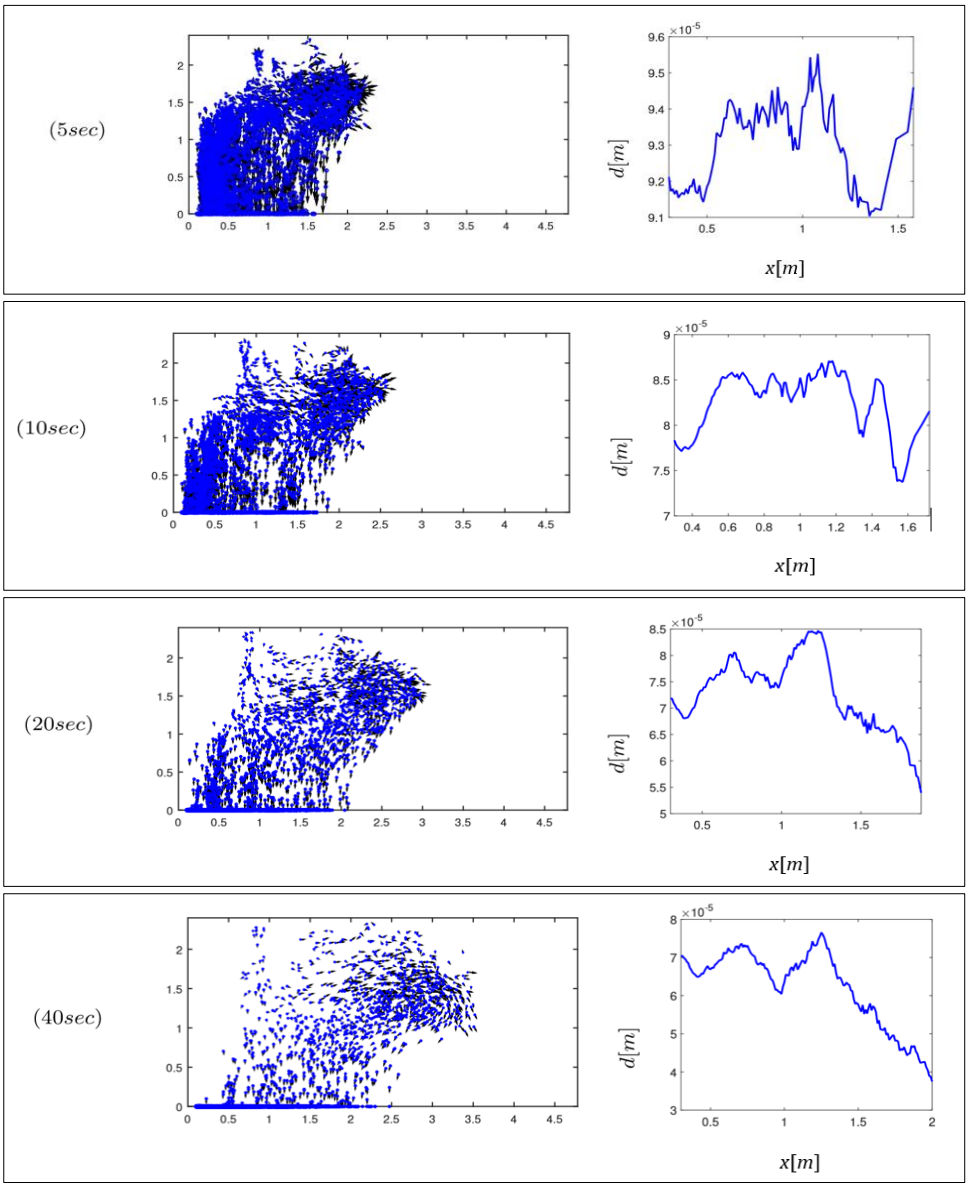

Figure 9. On the left panel, Cough drops a 2D velocity vector in an x-z plane. On the right panel, the average size of the drops deposited on the ground with respect to the horizontal distance to the mouth

Bourouiba reported that after the sneeze, a turbulent cloud is formed, and the smaller droplets are trapped in the turbulent puff cloud, remain suspended, can travel the dimensions of a room, and land up to 6 to 8 m away. Figure 10 shows that the same phenomenon occurs for the cough. At the tip of the cough jet, a semi-spherical cloud is formed, and thousands of smaller particles are trapped inside it. These particles rotate around the center of the cloud while moving forward and expanding. The high streamwise velocity of this cloud leads to its separation from the heavier droplets that are falling. This rotating cloud can travel up to 5 meters and hit the front wall. This phenomenon challenges the 1-2 meter recommended social distancing if two persons stay in front of each other for some time. In Figure 9, it is seen that for a time higher than only 10 seconds, the cough drops travel more than 2.5 meters. This observation brings a reconsideration for social distancing in a situation where people have interacted with others for a longer time, such as being in a meeting or waiting room.

In the second study, the spreading of the virus in a confined room is investigated. Two scenarios are studied. For case (1), the room is completely confined by the walls, and there is no ventilation. In case (2), there is an open window that could ventilate the aerosols out of the room. Table 1 and Figure 11 compare the percentage of cough drops on the ground, in the air, and ventilated through the windows for the open and closed windows for 5 minutes after the cough.

For the completely closed room (no window), about 93% of the droplets deposit on the ground, but about 7% of total particles remain in the air even 5 minutes after the cough. By opening the window, the drops start to get ventilated out of the windows 50 seconds after the cough. Two minutes after the cough, almost all droplets have been ventilated (Figures 11 and 12), and there are no drops remaining in the air. Figure 13 shows the cough drops spreading and ventilating in a room with an open window. It is seen that only one minute after the drop, the small droplets ($d < 20\mu$) have become aerosols, and the low airflow due to the AC circulates these aerosols in the entire room. But these aerosols slowly exit through the window, and after five minutes, very few remain in the room. This comparison shows the dangers of staying in a room with a closed window and no ventilation. Public places such as doctor waiting rooms, work meetings, hair salons, and many other places where people need to stay with others for a long period of time in confined rooms could potentially be high-risk areas, and it is crucial to keep the windows open for ventilation of the respiratory droplets.

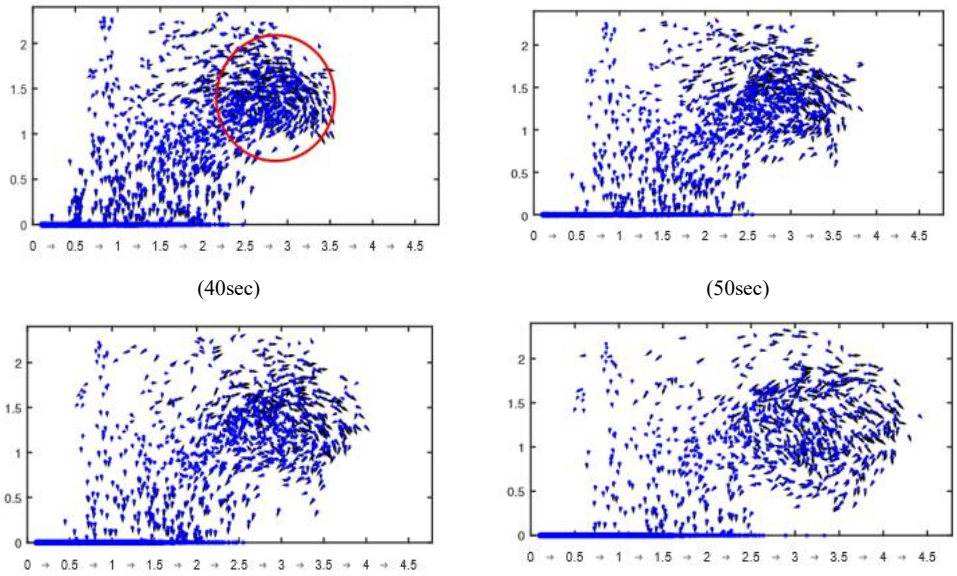

Figure 10. **Trapped particles in the cloud of the flow**

Table 1. **Comparison of cough drops percentages landed on the ground, suspended in the air and ventilated through the window**

Particle Percentage	On The Ground	In The Air	Ventilated Through The Window
Window closed	93.3	6.7	-
Window open	86.3	0.97	12.7

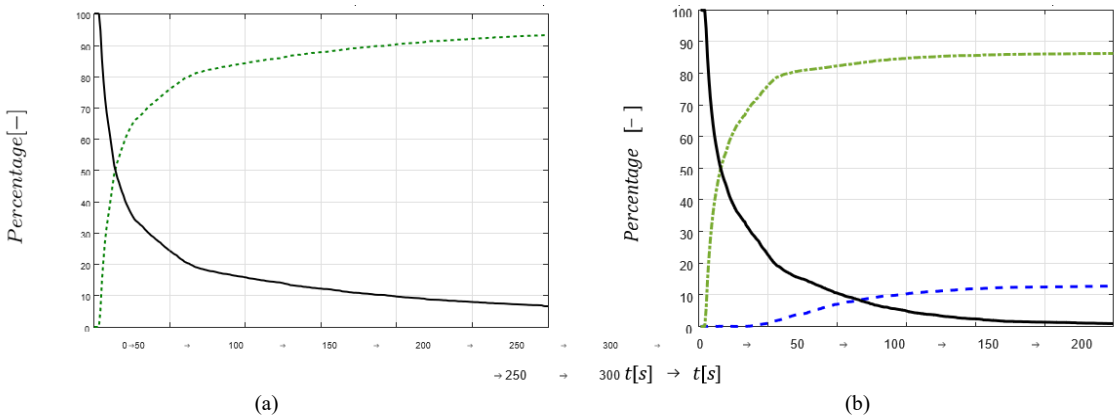

Figure 11. **(a) Percentage of the number of drops floating in the room ( ), deposited on the ground ( ) and ventilated through the window(---) with respect to the total number of cough drops, (b) No window, Open window**

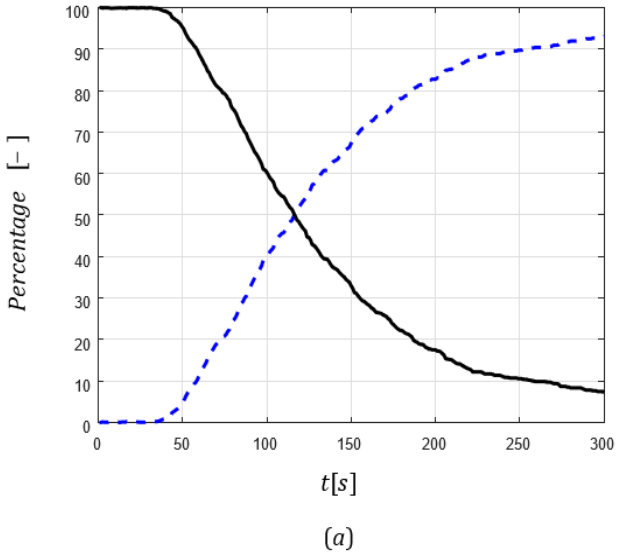

Figure 12. Percentage of the number of drops floating in the room ( ) and ventilated through the window(---) withrespecttosummationofdropsfloatinginroomandventilatedthroughthewindow

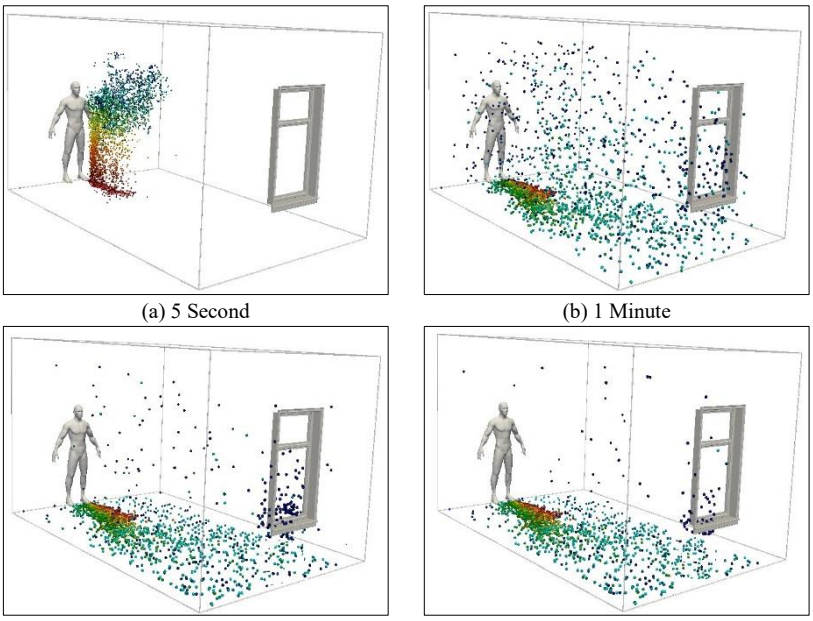

(a) 5 Second (b) 1 Minute

(c) 3 Minutes (d) 3 Minutes

Figure 13. Aerosols spread and ventilate in a room with an open window; droplets are colored by their size

5. Conclusion

In this paper, the study of cough flow and the spreading of cough droplets have been investigated. First, the capability of the flow solver was validated by comparing the velocity field with experimental data. Then, the propagation of the drops was studied. It was found that the droplets could spread far beyond the social distancing protocols if the persons were standing in front of each other. Furthermore, a small air flow circulation in the room could potentially spread the virus in the entire room only after 1 minute after the cough. In the case of no ventilation, the majority of these drops deposit on the ground, but around 7% of them become aerosols and circulate in the room, which might transmit the disease if they contain the virus. However, by opening the window, the droplets start to be ventilated, and after 5 minutes, less than 1% stay in the room, and almost all of them fall on the ground or exit through the window. In summary, this study emphasizes the importance of room ventilation and maintaining social distancing (more than 4 meters) for controlling the current COVID-19 pandemic or any other pandemic in the future.

6. References

[1] Morgenstern, J. (2020). Aerosols, Droplets, and Airborne Spread: Everything you could possibly want to know. First10EM Blog. doi:10.51684/firs.17317.

[2] Yan, J., Grantham, M., Pantelic, J., Bueno de Mesquita, P. J., Albert, B., Liu, F., Ehrman, S., Milton, D. K., Adamson, W., Beato-Arribas, B., Bischoff, W., Booth, W., Cauchemez, S., Ehrman, S., Enstone, J., Ferguson, N., Forni, J., Gilbert, A., … Tellier, R. (2018). Infectious virus in exhaled breath of symptomatic seasonal influenza cases from a college community. Proceedings of the National

Academy of Sciences, 115(5), 1081–1086. doi:10.1073/pnas.1716561115.

[3] Asadi, S., Wexler, A. S., Cappa, C. D., Barreda, S., Bouvier, N. M., & Ristenpart, W. D. (2019). Aerosol emission and superemission during human speech increase with voice loudness. Scientific Reports, 9(1), 9 2348 ,. doi:10.1038/s41598-019-38808-z.

[4] Chao, C. Y. H., Wan, M. P., & Sze To, G. N. (2008). Transport and removal of expiratory droplets in hospital ward environment. Aerosol Science and Technology, 42(5), 377–394. doi:10.1080/02786820802104973.

[5] Beans, C. (2020). Fluid dynamics work hints at whether spoken word can spread COVID-19. National Academy of Sciences, Washington, United States.

[6] Tellier, R. (2009). Aerosol transmission of influenza A virus: A review of new studies. Journal of the Royal Society Interface, 6(SUPPL. 6), 783– 790,. doi:10.1098/rsif.2009.0302.focus.

[7] Stetzenbach, L. D., Buttner, M. P., & Cruz, P. (2004). Detection and enumeration of airborne biocontaminants. Current Opinion in Biotechnology, 15(3), 170–174. doi:10.1016/j.copbio.2004.04.009.

[8] Bourouiba, L. (2016). A Sneeze. New England Journal of Medicine, 375(8), e15. doi:10.1056/nejmicm1501197.

[9] Nicas, M., Nazaroff, W. W., & Hubbard, A. (2005). Toward Understanding the Risk of Secondary Airborne Infection: Emission of Respirable Pathogens. Journal of Occupational and Environmental Hygiene, 2(3), 143–154. doi:10.1080/15459620590918466.

[10] Lindsley, W. G., Pearce, T. A., Hudnall, J. B., Davis, K. A., Davis, S. M., Fisher, M. A., Khakoo, R., Palmer, J. E., Clark, K. E., Celik, I., Coffey, C. C., Blachere, F. M., & Beezhold, D. H. (2012). Quantity and size distribution of cough-generated aerosol particles produced by influenza patients during and after illness. Journal of Occupational and Environmental Hygiene, 9(7), 443–449. doi:10.1080/15459624.2012.684582.

[11] Morawska, L. (2006). Droplet fate in indoor environments, or can we prevent the spread of infection? Indoor Air, 16(5), 335–347. doi:10.1111/j.1600-0668.2006.00432.x.

[12] Cowling, B. J., Ip, D. K. M., Fang, V. J., Suntarattiwong, P., Olsen, S. J., Levy, J., Uyeki, T. M., Leung, G. M., Malik Peiris, J. S., Chotpitayasunondh, T., Nishiura, H., & Mark Simmerman, J. (2013). Aerosol transmission is an important mode of influenza A virus spread. Nature Communications, 4. doi:10.1038/ncomms2922.

[13] Kang, Z., Zhang, Y., Fan, H., & Feng, G. (2015). Numerical Simulation of Coughed Droplets in the Air-Conditioning Room. Procedia Engineering, 121, 114–121. doi:10.1016/j.proeng.2015.08.1031.

[14] Pendar, M.-R., & Páscoa, J. C. (2020). Numerical modeling of the distribution of virus carrying saliva droplets during sneeze and cough. Physics of Fluids, 32(8). doi:10.1063/5.0018432.

[15] Fiegel, J., Clarke, R., & Edwards, D. A. (2006). Airborne infectious disease and the suppression of pulmonary bioaerosols. Drug Discovery Today, 11(1–2), 51–57. doi:10.1016/s1359-6446(05)03687-1.

[16] Scharfman, B. E., Techet, A. H., Bush, J. W. M., & Bourouiba, L. (2016). Visualization of sneeze ejecta: steps of fluid fragmentation leading to respiratory droplets. Experiments in Fluids, 57(2), 1–9. doi:10.1007/s00348-015-2078-4.

[17] Gupta, J. K., Lin, C.-H., & Chen, Q. (2009). Flow dynamics and characterization of a cough. Indoor Air, 19(6), 517–525. doi:10.1111/j.1600-0668.2009.00619.x.

[18] Tölke, J. (2008). Implementation of a Lattice Boltzmann kernel using the Compute Unified Device Architecture developed by nVIDIA. Computing and Visualization in Science, 13(1), 29–39. doi:10.1007/s00791-008-0120-2.

[19] Elghobashi, S. (1994). On predicting particle-laden turbulent flows. Applied Scientific Research, 52(4), 309–329. doi:10.1007/BF00936835.

[20] Maxey, M. R., & Riley, J. J. (1983). Equation of motion for a small rigid sphere in a nonuniform flow. Physics of Fluids, 26(4), 883–889. doi:10.1063/1.864230.

[21] Lekien, F., & Marsden, J. (2005). Tricubic interpolation in three dimensions. International Journal for Numerical Methods in Engineering, 63(3), 455–471. doi:10.1002/nme.1296.

[22] Qian, Y. H., D'Humières, D., & Lallemand, P. (1992). Lattice BGK Models for Navier-Stokes Equation. Europhysics Letters (EPL), 17(6), 479–484. doi:10.1209/0295-5075/17/6/001.

[23] Yu, D., Mei, R., Luo, L.-S., & Shyy, W. (2003). Viscous flow computations with the method of lattice Boltzmann equation. Progress in Aerospace Sciences, 39(5), 329–367. doi:10.1016/s0376-0421(03)00003-4.

[24] Banari, A., Gehrke, M., Janßen, C. F., & Rung, T. (2020). Numerical simulation of nonlinear interactions in a naturally transitional flat plate boundary layer. Computers & Fluids, 203, 104502. doi:10.1016/j.compfluid.2020.104502

[25] Dudalski, N., Mohamed, A., Mubareka, S., Bi, R., Zhang, C., & Savory, E. (2020). Experimental investigation of far-field human cough airflows from healthy and influenza-infected subjects. Indoor Air, 30(5), 966–977. doi:10.1111/ina.12680.

[26] Mohamed, A. F. A. (2017). Experimental measurements of far field cough airflows produced by healthy and influenza-infected human subjects. Master Thesis, The University of Western Ontario, London, Canada.